Check for updates

RESEARCH ARTICLE

ADVANCED FUNCTIONAL MATERIALS
www.afm-journal.de

Engineering Electronic Inductive Effect of Linker in Metal-Organic Framework Glass Toward Fast-Charging and Stable-Cycling Quasi-Solid-State Lithium Metal Batteries

Lichao Li, Guangshen Jiang, Kun Wang, Anping Yang, Tengfei Cao, Ourui Kong, Jijia Li, Junpeng Zhu, Jingang Zheng, Chengguo Sun, Lixiang Li, Fei Xu,* and Baigang An**

Metal-organic frameworks (MOFs) have been corroborated as promising quasi-solid-state electrolytes (QSSEs) matrix relying on their structural and compositional traits, while low Li$^+$ conductivity (σ_{Li^+}) still afflicts their further advances due to intense constraints from anions and large ionic resistance from the grain boundary. Herein, a combination strategy of simultaneous electronic engineering of linker and vitrification is adopted to optimize σ_{Li^+} for MOF-based QSSEs. The introduction of an electrophilic —Cl substituent in benzimidazole linker compels the electron to deviate from Zn^{2+} and modulates their charge distribution, which immobilizes bis(trifluoromethanesulfonyl)imide anions and thus boosts Li$^+$ transference number. Meanwhile, the vitrification endows ZIF-62 with the elimination of boundary resistance for high ionic conductivity. Consequently, —Cl-substituted glassy ZIF-62 containing Li salt (Cl-Li-G62) showcases a high σ_{Li^+} of 4.89×10^{-4} S cm^{-1} at 25 °C. Impressively, Li metal batteries pair with LiFePO$_4$ cathode and Cl-Li-G62 present an initial capacity of 145.4 mAh g^{-1} with a decay rate of 0.006% at 1C, and a superior rate performance of 79.5 mAh g^{-1} at 5C. The work demonstrates the effectiveness of introducing electron-withdrawing groups into MOF glass for enhancing σ_{Li^+} and offers a strategy to boost fast-charging and stable cycling performance of MOF glass-based quasi-solid-state lithium metal batteries.

1. Introduction

With the ever-growing demands for high-energy-density yet outstanding-safety battery technology, solid-state lithium metal batteries (SLMBs) are undergoing blooming development owing to the inherent advantages of high theoretical capacity (3860 mAh g^{-1}) and low redox potential (−3.04 V vs the standard hydrogen electrode) of Li metal and the non-flammable nature of solid electrolytes.[1] Despite these advantages, unfortunately, the state-of-the-art SLMBs still suffer from several scientific hurdles that severely preclude practical applications. The major issues include the inferior fast-charging ability and long-term stability due to the sluggish cation conduction and aggravated dendrites originating from worse compatibility between the electrode/solid-state electrolyte.[2] Metal-organic frameworks (MOFs), constructed by organic ligands and metal ions, provide emerging platforms for exploring SSEs for their excellent insulation, well-defined structures, and high modularity.[3] Currently, MOFs such as ZIF-8,[4] HKUST-1,[5] UiO-66,[6] MIL-101[7] and MOF-74,[8] etc., were employed as SSE substrate and indeed showed high conductivity (σ) of 10^{-4} S cm^{-1}, even up to 10^{-3} S cm^{-1} in the presence of plasticizer/ionic liquid.[9] Nevertheless, Li$^+$ often contributes less to the overall ionic conductivity.[10] In this regard, Li$^+$ transference number (t_{Li^+}), defined as the contribution fraction of electric quantity from cation migration, is employed as an important index to evaluate Li$^+$ conduction behavior. Obviously, the simultaneously high σ and large t_{Li^+} are vital to manifest the effective sole cationic Li$^+$ conductivity (σ_{Li^+}, estimated by the σ multiplied by t_{Li^+}),[11] which thus closely associates with the fast-charging capability and cycling stability affected by the dendrite growth issue and unstable Li anode interphases. Despite high σ in MOF-based electrolytes, especially with the plasticizer/ionic liquid addition, the low t_{Li^+} (<0.5)[5,12] generally gives rise to worse σ_{Li^+}, mainly owing to the bulky solvation sheath around Li$^+$ with intense restraint. The t_{Li^+} values can be enhanced via solvation structure modulation by MOF pore structure, but the values are less than 0.7.[13] Vice versa, a few cases reported superior t_{Li^+}, while the low σ still restricts the enhancement of σ_{Li^+} for MOF-based electrolytes.[11a,14] To the best of our knowledge, the inferior σ_{Li^+} (<4.5×10^{-4} S cm^{-1})[15] in MOF-based electrolytes becomes a bottleneck to make a significant advancement in

---

L. Li, G. Jiang, K. Wang, O. Kong, J. Li, J. Zhu, J. Zheng, C. Sun, L. Li, B. An
School of Chemical Engineering
University of Science and Technology Liaoning
Anshan 114051, P. R. China
E-mail: jianggsh@ustl.edu.cn; bgan@ustl.edu.cn

A. Yang, T. Cao, F. Xu
State Key Laboratory of Solidification Processing
School of Materials Science and Engineering
Northwestern Polytechnical University
Xi'an 710072, P. R. China
E-mail: feixu@nwpu.edu.cn

C. Sun
School of Chemical Engineering
Nanjing University of Science and Technology
Nanjing, Jiangsu 210094, P. R. China

The ORCID identification number(s) for the author(s) of this article can be found under https://doi.org/10.1002/adfm.202505700

DOI: 10.1002/adfm.202505700

© 2025 Wiley-VCH GmbH

fast-charging capability and high capacity retention. Moreover, most of the C-rate performance in MOF-based electrolyte is lower than 75 mAh g^{-1} at 5C until now. Consequently, it is pressing to explore novel MOF-based quasi-solid-state electrolytes (QSSEs) to achieve both simultaneously superior σ and $t_{Li}{}^{+}$ to further boost the fast-charging performance and cycling stability of SLMBs.

In contrast with the crystalline MOFs, their glassy counterparts emerge as a brand-new member of the glass family after silicate glass, organic glass, and metal glass.[16] MOF glasses stand out as promising QSSEs among crystalline counterparts, resulting from the homogeneous ionic migration rate and the absence of grain boundary impedance.[17] These structural advantages of MOF glass on ionic conduction resemble sulfide and halide glass electrolytes.[18] Compared with sulfide glass electrolytes, MOF glass-based electrolytes have overwhelming air and humidity stability.[19] Our group pioneeringly ushered the application of ZIF-4 glass electrolyte in SLMBs.[3b] Subsequently, ZIF-62 glass-based electrolytes were also exploited[20] and our group recently discovered “relay race” style Li^+ conduction behavior with fast migration kinetics,[19] while their $\sigma_{Li}{}^{+}$ were also lower than 4.5×10^{-4} S cm^{-1} because of either inferior σ or poor $t_{Li}{}^{+}$ induced by the weak interactions between anions of Li salts and MOF glass substrate. Electronic structural regulation at the molecular level has been corroborated as an effective approach to achieve higher $t_{Li}{}^{+}$, while the grain boundary in crystalline MOF hinders further boosting σ.[13] Therefore, the simultaneous enhancement of σ and $t_{Li}{}^{+}$ to achieve higher $\sigma_{Li}{}^{+}$ ($>4.5 \times 10^{-4}$ S cm^{-1}) is the ideal solution yet challenging for MOF-based electrolytes. Intriguingly, elaborately engineering the electronic indcutive effect of linkers in vitrified MOFs is highly promising to further raise $\sigma_{Li}{}^{+}$ for promoting the fast-charging performance and cycling stability of SLMBs.

Herein, we fabricate the vitrified ZIF-62 with —Cl electron-withdrawing substituent, i.e., glassy Cl-ZIF-62 (denoted as Cl-G62) for SLMBs. Owing to the presence of a strongly electron-capturing —Cl group, the distorted electronic structure of Zn^{2+} node in Cl-G62 intensifies the electrostatic attraction with bis(trifluoromethanesulfonyl)imide anion ($TFSI^-$) from LiTFSI and thus enhances the $t_{Li}{}^{+}$. Meanwhile, the isotropy and boundary-free attributes of MOF glass permit high σ. As anticipated, $\sigma_{Li}{}^{+}$ of glassy Cl-Li-G62 reaches up to 4.89×10^{-4} S cm^{-1} at 25 °C, higher than those of the vitrified control samples H-Li-G62 (—H substituent) and NH_2-Li-G62 (—NH_2 substituent) and previously reported MOF-based electrolytes. As a consequence, the Cl-Li-G62 full cell paired with $LiFePO_4$ (LFP) releases 79.5 mAh g^{-1} at 5C. As for long-cycling performance, high incipient capacities of 145.4 mAh g^{-1} at 1C and 116.3 mAh g^{-1} at 3C with ultrahigh capacity retentions are achieved for Cl-Li-G62, superior to those of H-Li-G62 and NH_2-Li-G62. Our work verifies the effectiveness of simultaneously introducing an electron-withdrawing group and vitrifying MOF for synergistically boosting $\sigma_{Li}{}^{+}$, which propels the implementation of MOF glass-based electrolyte in SLMBs.

2. Results and Discussion

For vitrified MOFs, the physicochemical properties, including ionic conductivity, depend on their linkers, metal ion nodes, and the linker-metal node coordination.[21] Evidently, they are also dominated by electron-inductive effects from linkers. To clearly exhibit the above effects, the electrostatic potentials of the asymmetric units of R-G62 (R = —Cl, —H, and —NH_2; electronegativity order: —Cl > —H > —NH_2) are analyzed. To simplify the calculation, the building unit models with the formula of $Zn[R\text{-}bIm_{0.25}Im_{1.75}]$ (R-G62, bIm = benzimidazole, Im = imidazole) were extracted and saturated with hydrogen atoms in **Figure 1a**. Blue color present in the isosurface of electrostatic potential stands for intensive electron-withdrawing property (electrophilicity), and red color represents strong electron-donating ability (nucleophilicity). For Cl-G62, the —Cl electron-capturing group displays a strong green color, and the central Zn^{2+} domain takes on a dense red color. These results mean that —Cl in 5-chlorobenzimidazole can deflect the electron cloud from Zn^{2+} through robust electron capture along d-π and π–π conjugation structures.[22] With the locally distorted positive charge distribution, Zn^{2+} node intensively traps more $TFSI^-$ through electrostatic interaction, as is illustrated in Figure 1b. This situation loosens the ion pairing interaction between Li^+ and $TFSI^-$, thus boosting Li^+ mobility. On the contrary, the —NH_2 group showcases red color, and Zn^{2+} displays yellow color in NH_2-G62, which implies that the —NH_2 electrophobic substituent in the linker renders the electron cloud to lean toward Zn^{2+}. The generated electron-donating inductive effect slightly impairs the interaction between $TFSI^-$ and Zn^{2+}. Correspondingly, Li^+ motion is slowed down due to the strong restriction from $TFSI^-$ anions. The feature of electrostatic potential in H-G62 is located between those of Cl-G62 and NH_2-G62. Theoretically, ionic conductivities in these three MOF glasses should obey the order: Cl-G62 > H-G62 > NH_2-G62.

According to the above theoretical analysis, three crystalline MOFs, i.e., Cl-ZIF-62, H-ZIF-62, and NH_2-ZIF-62, with varying electronegative substituents on the benzimidazole linker were initially synthesized. Actually, the crystalline Cl-ZIF-62 and NH_2-ZIF-C62 were first found by Thomas D. Bennett's group.[23] Herein, these three MOF crystals are uniformly named as Cl-C62, H-C62, and NH_2-C62 for better understanding. As for crystalline samples, their X-ray diffraction (XRD) patterns are parallel and in good agreement with that of the simulated ZIF-62 (**Figure 2a**), because Cl-C62, H-C62, and NH_2-C62 are affiliated with the ZIF-62 family.[24] They underwent the vitrification process, and the corresponding three MOF glasses of Cl-G62, H-G62, and NH_2-G62 were finally obtained. As an example, the main chemical materials involved in Cl-G62 preparation were tracked by a Fourier transform infrared (FTIR) spectrometer. In Figure 2b, the N—H band (3016 cm^{-1}) assigned to 5-chlorobenzimidazole and imidazole is absent, and Zn—N (427 cm^{-1}) band emerges in crystalline Cl-C62, indicative of the coordination occurrence between ligands and metal center.[3b] After vitrification, C═N (1597 cm^{-1}), C═C (1669 cm^{-1}), C—Cl (800 cm^{-1}) and Zn—N characteristic bands are still reserved for Cl-G62, corroborating the absence of chemical reaction during vitrification. A similar phenomenon also occurs to H-G62 and NH_2-G62 (Figures S1 and S2, Supporting Information). In ^1H NMR spectra, the peaks at 2.94 and 2.77 ppm, ascribed to *N*, *N*-dimethylformamide disappear (Figure S3, Supporting Information). The ^1H NMR peaks present in Cl-C62 are all retained in Cl-G62, but the peak at 4.61 ppm shifts to 4.50 ppm and becomes

© 2025 Wiley-VCH GmbH

16163028, 0, Downloaded from https://advanced.onlinelibrary.wiley.com/doi/10.1002/adfm.202505700 by Northwestern Polytechnic, Wiley Online Library on [29/05/2025]. See the Terms and Conditions (https://onlinelibrary.wiley.com/terms-and-conditions) on Wiley Online Library for rules of use; OA articles are governed by the applicable Creative Commons License

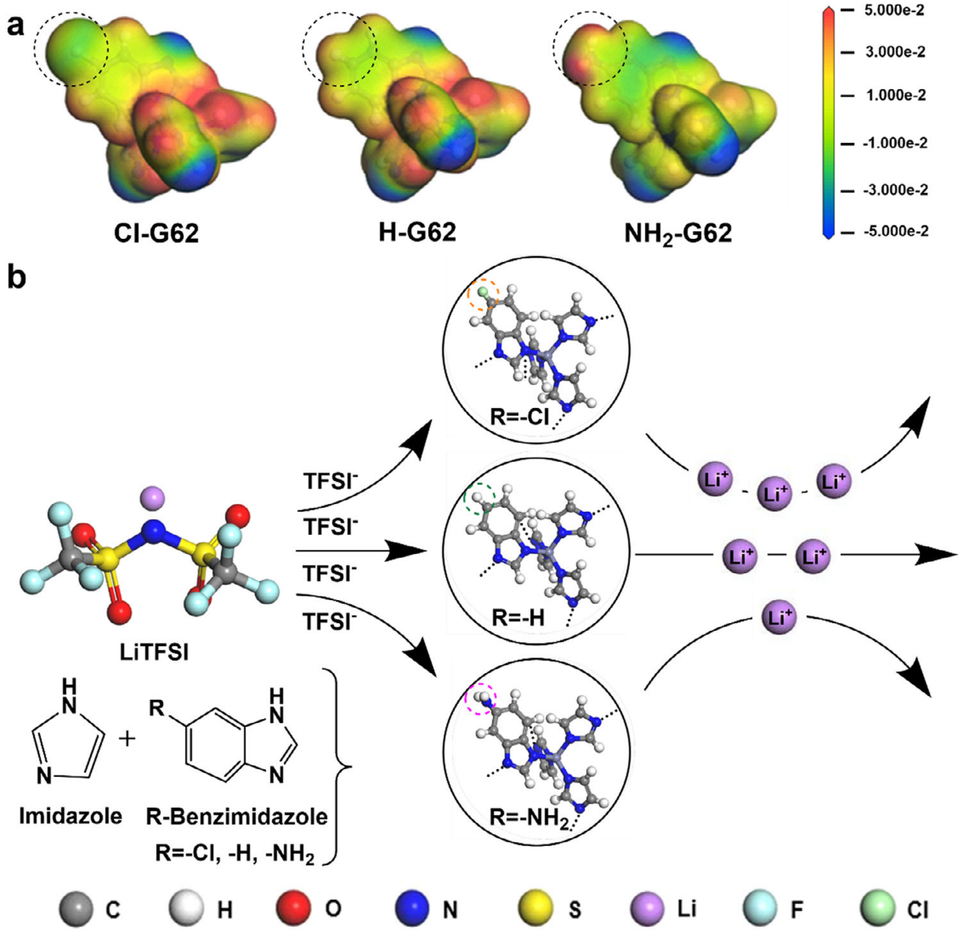

Figure 1. a) Isosurfaces of electrostatic potential of ZIF-62 glass from linker with varied substituents (R = —Cl, —H, —NH$_2$); b) Schematic of varied substituents effects on ionic conduction of Cl-G62, H-G62, and NH$_2$-G62.

broader, indicating a change of chemical coordination environment because of vitrification. After heat treatment, the three crystals have completely converted into amorphous counterparts, as verified by merely two broad peaks in their respective XRD patterns (Figure 2c). In the differential scanning calorimetry (DSC) curve of Cl-G62, the vitrification phenomenon with glass transition temperature (T_g) of 310 °C exists in the temperature-rise period (Figure 2d), suggesting that the as-obtained amorphous products are glassy materials.[23] As shown in Figure 2e and Figure S4 (Supporting Information), the vitrified Cl-G62 demonstrates deep brown bulk blocks due to fusion and is transparent with an irregular shape under an optical microscope. As revealed in scanning electron microscopy (SEM) images and energy dispersive spectra (EDS) mappings (Figure 2f), the well-distributed C, N, Zn, and Cl elements are detected in Cl-G62. Likewise, the other H-G62 and NH$_2$-G62 glasses also present irregularly shaped blocks (Figures S5, S6, Supporting Information). Owing to the good endurance toward the elevated voltage of 200 kV,[25] high-resolution transmission electron microscopy (HRTEM) investigation was conducted to examine the microstructure of Cl-G62. The twisty textures rather than ordered lattices are clearly observed in HRTEM images (Figure 2g), suggesting the glassy structure of Cl-G62. Furthermore, the halo-like selected area electron diffraction (SAED) pattern also proves the existence of the glassy state.[26] CO$_2$ adsorption/desorption curves of these three samples showcase the respective Brunauer-Emmett-Teller (BET) surface areas of 254.5, 251.1, and 240.0 m^2 g^{-1} with micropores concentrated on 0.58, 0.59, and 0.53 nm for Cl-G62, H-G62, and NH$_2$-G62 (Figures S7–S9, Supporting Information), respectively. This low-porosity phenomenon is also found in previous literature and mainly arises from structural deformation and densification during vitrification, accompanying the dissociation of the Zn—N coordination bond and the exposure of open metal sites.[27]

These three vitrified MOFs were processed into electrolyte membranes (see the Supporting Information), and they are separately denoted as Cl-Li-G62, H-Li-G62, and NH$_2$-Li-G62. The electrolyte films present relatively dense but not coherent monoliths, and their thicknesses of them were controlled to ≈80 µm (Figures S10 and S11, Supporting Information). The determined liquid content is 19.42 wt.% by thermal gravimetric analysis (TGA) in Cl-Li-G62 film (Figure S12, Supporting Information). As an important index, the ionic conductivity of QSSE at room temperature is the first and foremost consideration. As portrayed in **Figure 3a**, these three electrolyte films show ionic resistances of 6.7, 8.9, and 9.7 Ω in ss|QSSE|ss (ss: stainless steel) cell for

© 2025 Wiley-VCH GmbH

16163028, 0, Downloaded from https://advanced.onlinelibrary.wiley.com/doi/10.1002/adfm.202505700 by Northwestern Polytechnic, Wiley Online Library on [29/05/2025]. See the Terms and Conditions (https://onlinelibrary.wiley.com/terms-and-conditions) on Wiley Online Library for rules of use; OA articles are governed by the applicable Creative Commons License

16163028, 0, Downloaded from https://advanced.onlinelibrary.wiley.com/doi/10.1002/adfm.202505700 by Northwestern Polytechnic, Wiley Online Library on [29/05/2025]. See the Terms and Conditions (https://onlinelibrary.wiley.com/terms-and-conditions) on Wiley Online Library for rules of use; OA articles are governed by the applicable Creative Commons License

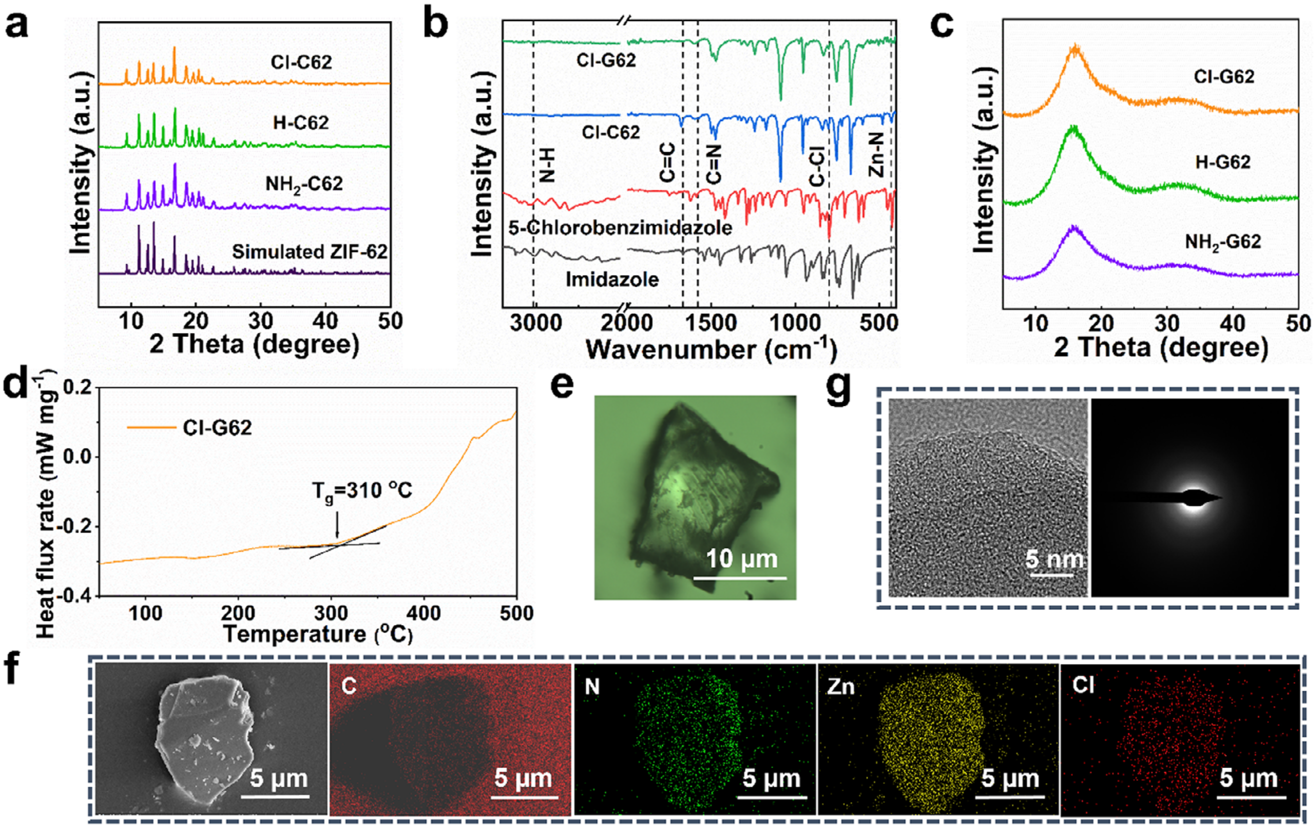

Figure 2. a) XRD patterns of ZIF-62 with varied substituents (R = —Cl, —H, —NH_2) and simulated ZIF-62; b) FTIR spectra of imidazole, 5-chlorobenzimidazole, Cl-C62 and Cl-G62; c) XRD patterns of Cl-G62, H-G62 and NH_2-G62; d) DSC upscan of Cl-G62; e) Optical microscopy image of Cl-G62 block; f) SEM image of Cl-G62 and its EDS mappings of C, N, Zn and Cl elements; g) HRTEM images of Cl-G62 with its SAED pattern.

Cl-Li-G62, H-Li-G62, and NH_2-Li-G62 at 25 °C according to electrochemical impedance spectroscopy (EIS) measurements. The corresponding conductivities are separately 6.11×10^{-4}, $4.59 \times 10^{-4,}$ and 4.21×10^{-4} S cm^{-1}, in agreement with the electronegativity sequence of the substituents. Compared with the previous reports, in reality, the ionic conductivities of H-Li-G62 and NH_2-Li-G62 at 25 °C are already relatively high, resulting from the grain boundary-free and isotropy attributes of the glass phase.[20a] As for Cl-Li-G62, it has higher ionic conductivity derived from the fact that the high electronegativity of the —Cl electron-withdrawing group despoils electrons from Zn^{2+}, apart from the existing glassy features.[28] The ionic conductivities of Cl-G62 with various ClbIm/Im ratio (i.e., Zn[$ClbIm_{0.35}Im_{1.65}$] and Zn[$ClbIm_{0.05}Im_{1.95}$]) and ZIF-4-$CN_{0.29}$ glass were determined to be 6.87×10^{-4}, 5.24×10^{-4} and 6.98×10^{-4} S cm^{-1}, further validating the ionic conductivity with close association with electron-withdrawing group (Figures S13–S16, Supporting Information). Nyquist plots at various temperatures are revealed in Figures S17–S19 (Supporting Information), and the corresponding ionic resistances decrease with increasing temperature for all electrolytes. A linear relationship between logarithmic ionic conductivities and the reciprocals of thermodynamic temperature, obeying the Arrhenius equation, is presented in Figure 3b. Representing migration barrier in SSE, the activation energy (E_a) can be calculated from the slope of the fitted line according to the Arrhenius equation. The calculated E_a value of Cl-Li-G62 is 0.14 eV, slightly lower than those of H-Li-G62 (e.g., 0.16 eV) and NH_2-Li-G62 (e.g., 0.18 eV). The lowest E_a of Cl-Li-G62 also illuminates the dual effects from the electron-withdrawing effect and the attributes of MOF glass on Li^+ conduction.

As is well known, $t_{Li}{}^+$ directly reflects cation migration ability and polarization degree when the batteries are running. Figure 3c reveals that Cl-Li-G62 has the highest $t_{Li}{}^+$ of 0.80 in contrast with H-Li-G62 (e.g., 0.71) and NH_2-Li-G62 (e.g., 0.31) (Figures S20–S22, Supporting Information), hinting at the fastest Li^+ transfer kinetics and the lowest polarization degree of Cl-Li-G62, substantiated as below. Such $t_{Li}{}^+$ enhancement of Cl-Li-G62 originates from the presence of —Cl electron-withdrawing group, which further attracts the charge of Zn^{2+}, intensifying the chemical interaction with $TFSI^-$ and alienates Li^+.[14a,b] To elucidate the underlying mechanisms of the above results, binding energy (BE) between $TFSI^-$ and the simplified structures representing the three MOF glasses was calculated based on the density functional theory (DFT) simulations. As seen from Figure 3d, Cl-G62 shows the highest BE of 3.88 eV in contrast with H-G62 (3.22 eV) and NH_2-G62 (2.00 eV). The strong interactions between $TFSI^-$ and Cl-G62 are also validated by O 1s spectra with a large amount of —S=O...Zn^{2+} species (532.5 eV) in Figure S23 (Supporting Information). This suggests that the deflected electronic structure of Zn^{2+} induced by electrophilic substituent intensely anchors $TFSI^-$ anions and thus promotes Li^+ motion.

© 2025 Wiley-VCH GmbH

16163028, 0, Downloaded from https://advanced.onlinelibrary.wiley.com/doi/10.1002/adfm.202505700 by Northwestern Polytechnic, Wiley Online Library on [29/05/2025]. See the Terms and Conditions (https://onlinelibrary.wiley.com/terms-and-conditions) on Wiley Online Library for rules of use; OA articles are governed by the applicable Creative Commons License

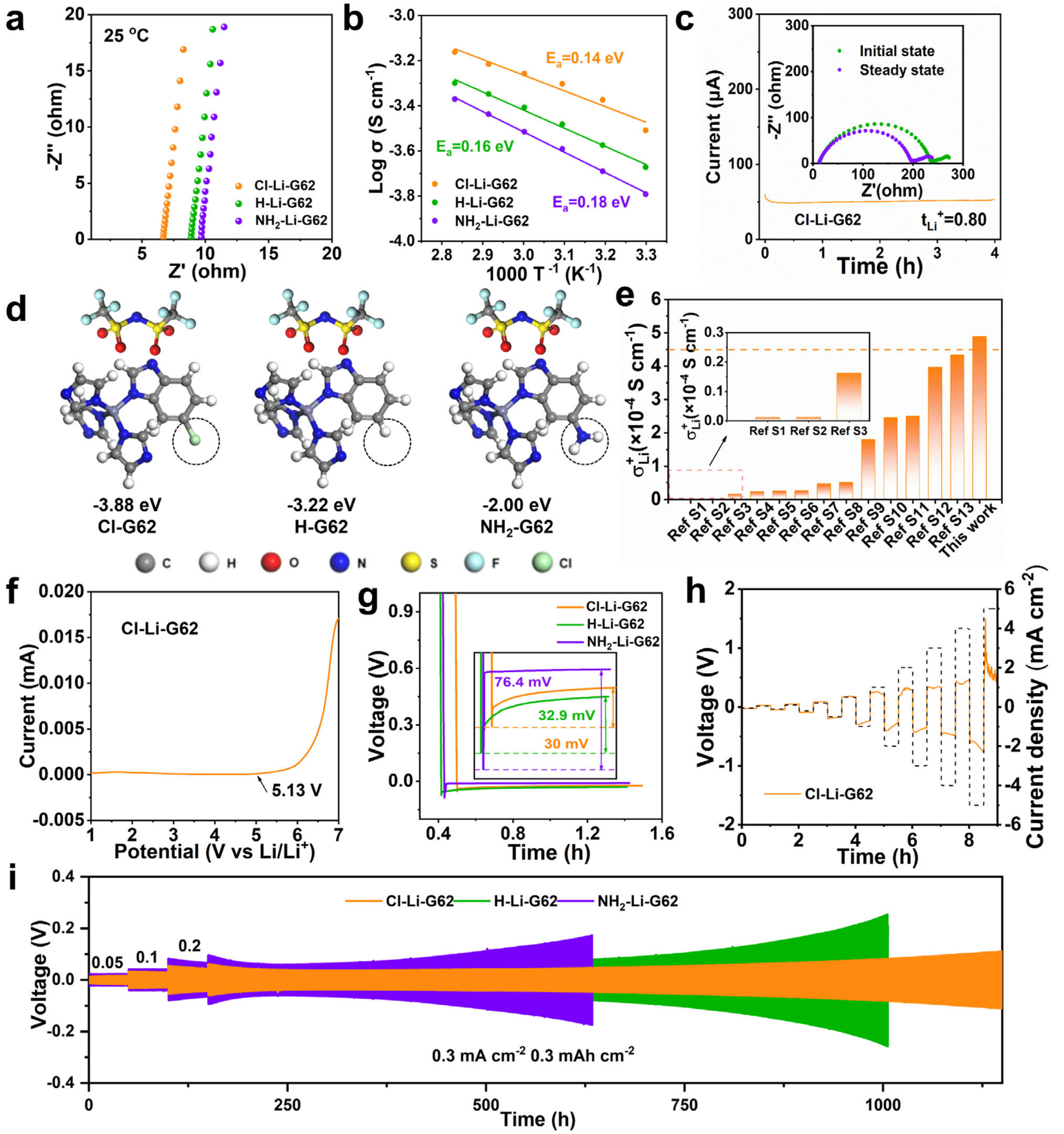

Figure 3. a) Nyquist plots at 25 °C and (b) Temperature-dependent conductivity plot of Cl-Li-G62, H-Li-G62 and NH_2-Li-G62; c) Current-time curves of Li|Cl-Li-G62|Li symmetric cells (inset: EIS at initial and steady states); d) Binding energies of $TFSI^-$ with Cl-G62, H-G62 and NH_2-G62; e) $\sigma_{Li}{}^+$ comparisons of the reported MOF-based electrolytes and Cl-Li-G62; f) LSV of Li|Cl-Li-G62|ss cell; g) Voltage profiles of Li|QSSE|Cu; h) Voltage response at various current densities and (i) cycling stability of Li plating/stripping for Li|QSSE|Li symmetric cells.

As to the effective conductivity, the highest $\sigma_{Li}{}^+$ of 4.89×10^{-4} S cm^{-1} for Cl-Li-G62 is displayed in comparison with H-Li-G62 (3.26×10^{-4} S cm^{-1}) and NH_2-Li-G62 (1.31×10^{-4} S cm^{-1}). We also compared $\sigma_{Li}{}^+$ of the previously reported MOF-based electrolytes, and our Cl-Li-G62 showcases the unparalleled $\sigma_{Li}{}^+$, as plotted in Figure 3e. A wide electrochemical stability window (ESW) is meaningful to enhance the energy density of batteries. In Figure 3f, Cl-Li-G62 reveals a wide ESW up to 5.13 V, which is comparable to H-Li-G62 and NH_2-Li-G62 (Figures S24 and S25, Supporting Information). This implies Cl-Li-G62 owns good antioxidation capability and can match with the high-voltage cathode. Li||Cu cells were assembled to investigate the effect

© 2025 Wiley-VCH GmbH

of different electrolytes on Li deposition behavior. As depicted in Figure 3g, Cl-Li-G62 displays a nucleation overpotential of 30.0 mV, slightly lower than that of H-Li-G62 (e.g., 32.9 mV). Especially, the nucleation overpotential of NH_2-Li-G62 is as high as 76.4 mV, elucidating that the electron-donating effect from linkers in the MOF glass electrolyte is adverse for Li deposition. The critical current density (CCD) is an index to assess the maximum current that SSE can tolerate. Cl-G62 and NH_2-G62 bear the same CCD values of 5 mA cm^{-2}, whereas H-G62 has a lower CCD of 4 mA cm^{-2}, as plotted in Figure 3h, Figures S26 and S27 (Supporting Information). Cl-Li-G62 has the lowest polarization voltage among these three glassy electrolytes. To compare stripping/plating kinetics of Li, Tafel plots of symmetric Li|QSSE|Li cells were recorded. The exchange current density (J_0) is 0.81 mA cm^{-2} for Cl-Li-G62, higher than those of H-Li-G62 (0.66 mA cm^{-2}) and NH_2-Li-G62 (0.61 mA cm^{-2}), as revealed in Figure S28 (Supporting Information), which accelerates interfacial charge transfer during stripping/plating processes.[29] To further probe the Li stripping/plating behavior and the compatibility between Li anodes and these three electrolytes, long cycling tests were also carried out in Li|QSSE|Li cells. At 0.2 mA cm^{-2} and 0.2 mAh cm^{-2}, Li|Cl-Li-G62|Li steadily operates for 1500 h and undergoes a slight increasing polarization without failure during the following 1250 h, while short circuit occurs when Li|H-Li-G62|Li and Li|NH_2-Li-G62|Li runs 2270 and 950 h, respectively (Figure S29, Supporting Information). After the initial activation of 0.05–0.2 mA cm^{-2}, Cl-Li-G62 undergoes a stable cycling with a polarization voltage of 37.6 mV for 750 h and then an increasing polarization process with 110.8 mV in the subsequent 350 h at 0.3 mA cm^{-2} and 0.3 mAh cm^{-2} (Figure 3i). In comparison, H-Li-G62 and NH_2-Li-G62 showcase larger polarization voltages of 247.6 and 167.8 mV after 850 and 480 h, respectively. Such a phenomenon illustrates that Cl-Li-G62 bears the outstanding modulation of Li deposition and remarkable compatibility with Li anode.[3b] As to flame retardance, Cl-Li-G62 cannot catch fire when approaching the flame within 3 s and presents a partial blackened film once withdrawn from the flame (Figure S30, Supporting Information). The presence of N species in imidazole and 5-chlorobenzimidazole from Cl-C62 can impede the combustion of Cl-Li-G62.[30] Therefore, the implementation of Cl-Li-G62 into SLMBs can boost their safety.

Encouraged by the superiority of Cl-Li-G62, the electrochemical performance of full cells matching different cathodes on the market was investigated. Rate capability, representing fast-charging ability, was analyzed first with LFP. LFP|Cl-Li-G62|Li delivers 166.3 mAh g^{-1} at 0.1C (1C = 170 mA g^{-1}), which is approaching the theoretical capacity of LFP (**Figure 4**a). Although these three samples have approximate capacities within the range of 0.1–0.5C, the capacity gaps are particularly evident under larger current densities. Especially, LFP|Cl-Li-G62|Li releases 79.5 mAh g^{-1} at 5C, markedly surpassing LFP|H-Li-G62|Li (e.g., 57.0 mAh g^{-1}) and LFP|NH_2-Li-G62|Li (e.g., 44.2 mAh g^{-1}). Impressively, the plateaus at 5C remain clearly discernible in the charge/discharge profiles of the Cl-Li-G62 cell (Figure S31, Supporting Information). We compared the rate performance disparity of UiO-66, Zn-MOF-74, NH_2-UiO-66, ZIF-4 glass, and ZIF-62 glass, etc., with that of Cl-Li-G62 paired with LFP. Our fabricated Cl-Li-G62 outperforms the best amongst the listed electrolytes, as shown in Figure 4b. The root of the above splendid performance is the prominent conductivity for cations resulting from electron-withdrawing effect plus the MOF glass attributes. As to long-term cyclability, Cl-Li-G62 cell displays a high initial capacity of 145.4 mAh g^{-1} with a capacity retention of 97.7% at 1C over 400 cycles, overmatching H-Li-G62 (e.g., 125.4 mAh g^{-1}) and NH_2-Li-G62 (e.g., 107.1 mAh g^{-1}) cells (Figure 4c). The capacity of Cl-Li-G62 is also superior to that of the reported MOF-based electrolytes, and the corresponding capacity decay rate is only 0.006%. Such a low fade rate is markedly lower than for other MOF-based electrolytes, apart from the higher capacity of Cl-Li-G62 (Figure 4d), validating the merits of such a composition design of MOF glass on cycling performance. Polarization voltage from the charge/discharge profiles of Cl-Li-G62 is 144 mV, evidently lower than those of H-Li-G62 (e.g., 187 mV) and NH_2-Li-G62 (e.g., 307 mV), as revealed in Figure S32 (Supporting Information). These results are consistent with Li|QSSE|Li symmetric cells. Under a higher current density of 3C, the cycling capacity of 111.9 mAh g^{-1} with a retention of 96.2% is delivered after 500 cycles for Cl-substituted ZIF-62 glass electrolyte (Figure 4e). The experimental group obviously overbalances H- and NH_2-substituted ZIF-62 glass SSEs with lower capacities of 76.5 and 56.0 mAh g^{-1} under the same conditions. Moreover, the corresponding Coulombic efficiency remains ≈100%, whether the current density is 1 or 3C. And the corresponding charge/discharge profiles of varied cycles nearly overlapped, further suggesting no evident capacity fade (Figures S33 and S34, Supporting Information).

The electrochemical performance of LFP|Cl-Li-G62|Li at high LFP loading is one of the important references to evaluate practical applications. At LFP loading of ≈13.2 mg cm^{-2}, LFP|Cl-Li-G62|Li runs 80 cycles with an incipient capacity of 140.6 mAh g^{-1} and a retention of 97.9% at 0.5C (Figure S35, Supporting Information). The cycling performance is better than that of some reported QSSEs (Table S1, Supporting Information). Amazingly, Cl-Li-G62 also exhibits admirable temperature adaptation. At −20 °C, the capacity of LFP|Cl-Li-G62|Li decays in the first 10 cycles and slowly increases to 79.0 mAh g^{-1} after 100 cycles at 0.1C (Figure S36, Supporting Information). At a higher temperature of 80 °C, it can discharge a high capacity of 169.3 mAh g^{-1} with a retention of 84.5% for 300 cycles at 1C (Figure S37, Supporting Information). Air stability is a crucial factor for SSE commercialization. After 7-day exposure in air, the XRD pattern of Cl-Li-G62 bears a resemblance to that of the fresh Cl-Li-G62 (Figure S38, Supporting Information). Once assembled in the cell, impressively, LFP|Cl-Li-G62|Li still functions well for 300 cycles with 119.7 mAh g^{-1} and a retention of 99.1% at 1C (Figure 4f), suggesting that our designed Cl-Li-G62 is insensitive to oxygen and humidity. Obviously, Cl-Li-G62 excels in air stability in comparison with oxide, sulfide, and halide electrolytes.[31] The excellent air stability of Cl-Li-G62 is of paramount significance for the scalable production, transport, and storage of SSE. Owing to the upper limit of ESW exceeding 5 V, high-voltage $LiNi_{0.8}Co_{0.1}Mn_{0.1}O_2$ (NCM 811) and $LiCoO_2$ (LCO) cathodes were also evaluated to confirm the feasibility of Cl-Li-G62. As showcased in Figure 4g, the NCM811|Cl-Li-G62|Li cell releases a capacity of 155.5 mAh g^{-1} with retention of 82.8% for 300 cycles under 1C after stepwise activation. When it comes to LCO, a capacity of 140.4 mAh g^{-1} is achieved for LCO|Cl-Li-G62|Li (Figure S39, Supporting Information). In short,

© 2025 Wiley-VCH GmbH

16163028, 0, Downloaded from https://advanced.onlinelibrary.wiley.com/doi/10.1002/adfm.202505700 by Northwestern Polytechnic, Wiley Online Library on [29/05/2025]. See the Terms and Conditions (https://onlinelibrary.wiley.com/terms-and-conditions) on Wiley Online Library for rules of use; OA articles are governed by the applicable Creative Commons License

16163028, 0, Downloaded from https://advanced.onlinelibrary.wiley.com/doi/10.1002/adfm.202505700 by Northwestern Polytechnic, Wiley Online Library on [29/05/2025]. See the Terms and Conditions (https://onlinelibrary.wiley.com/terms-and-conditions) on Wiley Online Library for rules of use; OA articles are governed by the applicable Creative Commons License

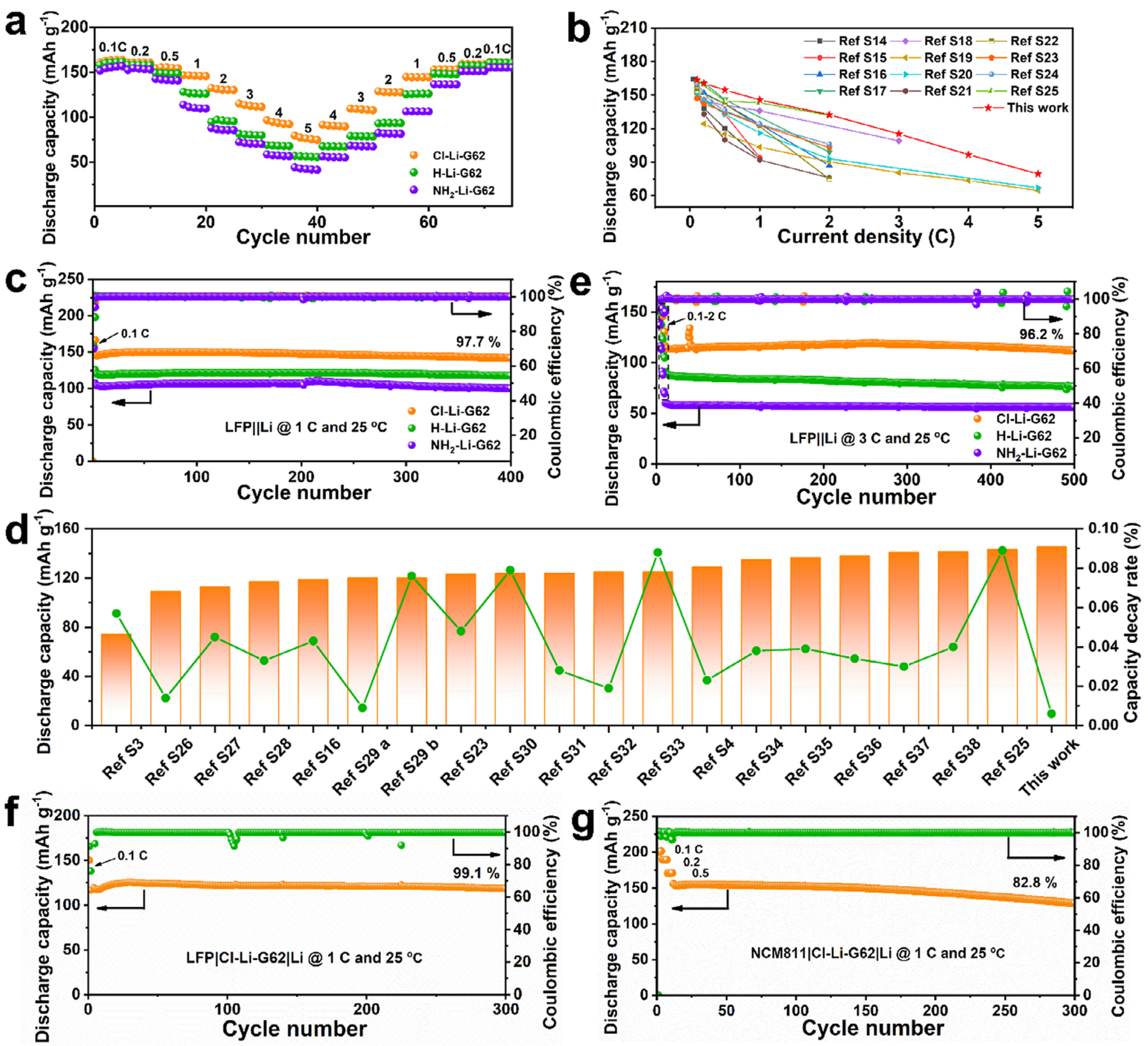

Figure 4. a) Rate performance of LFP|QSSE|Li; b) Rate performance comparisons of Cl-Li-G62 and the reported MOF-based electrolytes; c,e) Cycling stability of LFP|QSSE|Li at 1 and 3C; d) Comparisons of specific capacities at 1C and corresponding average capacity decay rate per cycle of various MOF-based electrolytes; f) Cycling performance of LFP|Cl-Li-G62|Li at 1C after 7-day exposure in air; g) Cyclability of NCM811|Cl-Li-G62|Li at 1C.

—Cl-modulated ZIF-62 glass displays the outstanding electrochemical performance.

To further investigate the origin of in electrochemical performance discrepancy, negative electrodes were meticulously analyzed. **Figure 5a** reveals the morphology of Li anodes in LFP|QSSE|Li after 50 cycles. SEM image of Li anode against Cl-Li-G62 shows a rather smooth and flat surface. In sharp contrast, Li anodes contacting with H-Li-G62 and NH_2-Li-G62 present evident wrinkles with relatively coarse surface, although the flatness of Li anodes in H-Li-G62 and NH_2-Li-G62 cells is comparable to those in the previously reported QSSEs because of the isotropy attribute of MOF glass.[3b,20b] The reason for the lower Li flatness in NH_2-Li-G62 with electrophobic group cells is ascribed to its low $t_{Li}{}^+$ due to the weak electrostatic interaction between Zn^{2+} with $TFSI^-$ and thus accelerate uneven Li nucleation. In the solid electrolyte interphase (SEI) film of Li anode from LFP|QSSE|Li, organic components contain $ROCO_2Li$ and RCO_2Li, as shown in C 1s and Li 1s X-ray photoelectron spectroscopy (XPS) data (Figure 5b), was derived from the decomposition of glycol dimethyl ether, propylene carbonate and Li salts. Organic component with a proper amount can increase the SEI resilience to mitigate volumetric fluctuation during charging/discharging,[32] but excess organic ingredients lower the ionic conductivity of the SEI layer due to the attribute of their segment motion. Apart from organic components, LiF and Li_2O inorganic components can be observed in Li 1s and F 1s

© 2025 Wiley-VCH GmbH

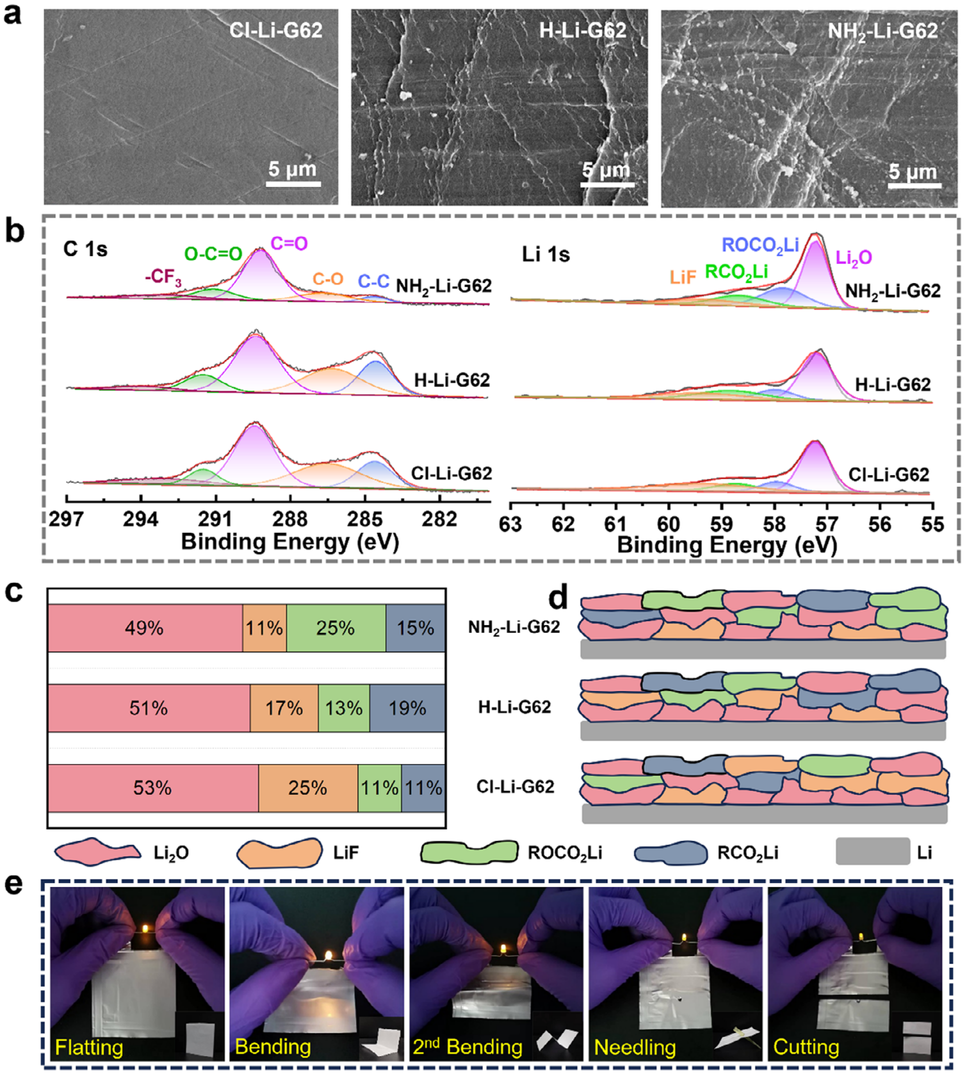

Figure 5. a) SEM images of Li anodes against Cl-Li-G62, H-Li-G62 and NH_2-Li-G62; b) C 1s, and Li 1s high-resolution XPS spectra of SEI layer on the cycled Li anodes; c) Composition content of LiF, Li_2O, $ROCO_2Li$ and RCO_2Li in three SEI layers in LFP|Cl-Li-G62|Li; d) the corresponding SEI composition models; e) Power supply of LFP|Cl-Li-G62|Li pouch cell under abuse conditions.

spectra (Figure 5b; Figure S40, Supporting Information). Although Li_2O contents in SEI layers are approximate for these three electrolytes, LiF content in Cl-Li-G62 significantly exceeds those of H-Li-G62 and NH_2-Li-G62 (Figure 5c). As previously reported, Li_2O can also facilitate cation conduction and enhance Coulombic efficiency.[33] The SEI properties, including ionic conductivity and anode protection, depend on the total content of Li_2O and LiF. The higher inorganic content, up to 78%, ensures faster Li^+ transfer in the SEI for the Cl-Li-G62 cell. This means that the SEI layer combines high ionic conductivity and rigidity from LiF and Li_2O, and the resilience of organic components.[34] The composition models of SEI for the three samples are portrayed in Figure 5d. The structural privilege of SEI film hinders its cracking and reconstruction, which is also conducive to high Coulombic efficiency and remarkable stability of the Li anode.[35] Combined with the advantages of SEI and Cl-Li-G62 electrolyte, the outstanding electrochemical performance can be achieved for the Cl-Li-G62 battery. To further illustrate the commercial potential and safety under abuse conditions of Cl-Li-G62, an LFP||Li pouch cell was assembled, equipped with Cl-Li-G62. As exhibited in Figure 5e, a pouch cell can still supply power for a light-emitting diode under bending, puncture, and cutting abuse conditions.

3. Conclusion

To summarize, we report modulating the electronic inductive effect of substituents on linkers and vitrification of MOF to optimize σ_{Li^+} for SLMBs. The introduced —Cl electron-withdrawing group in benzimidazole linker within ZIF-62 reinforces the distorted electron distribution of Zn^{2+}, where $TFSI^-$ anions from LiTFSI are intensively anchored through electrostatic interaction, and the alienated Li^+ gains much mobility in MOF glass. Additionally, the glass attributes reduce ionic transport resistance in

© 2025 Wiley-VCH GmbH

16163028, 0, Downloaded from https://advanced.onlinelibrary.wiley.com/doi/10.1002/adfm.202505700 by Northwestern Polytechnic, Wiley Online Library on [29/05/2025]. See the Terms and Conditions (https://onlinelibrary.wiley.com/terms-and-conditions) on Wiley Online Library for rules of use; OA articles are governed by the applicable Creative Commons License

glassy MOF. As we expected, Cl-Li-G62 showcases $\sigma_{\text{Li}}{}^{+}$ of 4.89 × 10^{-4} S cm^{-1} at 25 °C, surpassing most of MOF-based electrolytes. Benefiting from the above advantages, LFP|Cl-Li-G62|Li full cell delivers 145.4 and 79.5 mAh g^{-1} at 1 and 5C, respectively. Strikingly, Cl-Li-G62 displays outstanding air stability and still releases a high and steady capacity of 119.7 mAh g^{-1} at 1C after exposure in air. Introducing electron-withdrawing groups into MOF glass is a promising strategy to further enhance their $\sigma_{\text{Li}}{}^{+}$ and offer huge impetus for MOF glass-based solid-state lithium metal batteries.

Supporting Information

Supporting Information is available from the Wiley Online Library or from the author.

Acknowledgements

The funding from the National Natural Science Foundation of China (Nos. 52371224, 52322203, 52473220), the Talent Project Grants of the University of Science and Technology Liaoning (6003000341), and the Fundamental Research Funds of Education Bureau of Liaoning Province (JYTMS20230945) was gratefully acknowledged.

Conflict of Interest

The authors declare no conflict of interest.

Author Contributions

L.L. performed the material synthesis and electrochemical measurements. G.J. conceived the concept and designed the experiments. O.K., J.L., and J.Z. completed XRD and FTIR testing. T.C. was responsible for the theoretical calculations. J.Z. performed the SEM experiments. L.L., K.W. and A.Y. participated in material characterization. L.L. and G.J. wrote the draft. C.S., L.L., F.X., B.A., and G.J. revised the paper, supervised, and managed the entire experiment. All authors discussed the results and revised the manuscript.

Data Availability Statement

Research data are not shared.

Keywords

electron-withdrawing effect, lithium metal batteries, metal-organic frameworks, MOF glass, vitrification

Received: March 4, 2025
Revised: May 13, 2025
Published online:

---

[1] a) Y.-G. Lee, S. Fujiki, C. Jung, N. Suzuki, N. Yashiro, R. Omoda, D.-S. Ko, T. Shiratsuchi, T. Sugimoto, S. Ryu, J. H. Ku, T. Watanabe, Y. Park, Y. Aihara, D. Im, I. T. Han, *Nat. Energy* **2020**, *5*, 299; b) F. Ren, Y. Wu, W. Zuo, W. Zhao, S. Pan, H. Lin, H. Yu, J. Lin, M. Lin, X. Yao, T. Brezesinski, Z. Gong, Y. Yang, *Energy Environ. Sci.* **2024**, *17*, 2743.

[2] a) S. Duan, L. Qian, Y. Zheng, Y. Zhu, X. Liu, L. Dong, W. Yan, J. Zhang, *Adv. Mater.* **2024**, *36*, 2314120; b) H. L. Wan, J. J. Xu, C. S. Wang, *Nat. Rev. Chem.* **2024**, *8*, 30.

[3] a) J. Li, A. Kumar, S. Ott, *J. Am. Chem. Soc.* **2024**, *146*, 12000; b) G. Jiang, C. Qu, F. Xu, E. Zhang, Q. Lu, X. Cai, S. Hausdorf, H. Wang, S. Kaskel, *Adv. Funct. Mater.* **2021**, *31*, 2104300.

[4] J. Zhou, X. Wang, J. Fu, L. Chen, X. Wei, R. Jia, L. Shi, *Small* **2024**, *20*, 2309317.

[5] T. Wang, H. Yuan, H. Wang, Y. Guo, J. Yang, X. Liu, B. Liu, X. Wang, C. H. Kirk, J. Sun, Y.-W. Zhang, J. Wang, *Adv. Funct. Mater.* **2024**, *34*, 2405699.

[6] Y. Li, W. Chen, T. Lei, H. Xie, A. Hu, F. Wang, J. Huang, X. Wang, Y. Hu, C. Yang, J. Xiong, *Energy Storage Mater.* **2023**, *59*, 102765.

[7] R. Xu, S. Xu, F. Wang, R. Xiao, P. Tang, X. Zhang, S. Bai, Z. Sun, F. Li, *Small Struct.* **2023**, *4*, 2200206.

[8] P. P. Dong, X. H. Zhang, W. Hiscox, J. J. Liu, J. Zamora, X. Y. Li, M. Q. Su, Q. Zhang, X. F. Guo, J. McCloy, M. K. Song, *Adv. Mater.* **2023**, *35*, 2211841.

[9] a) A. E. Abdelmaoula, J. Shu, Y. Cheng, L. Xu, G. Zhang, Y. Xia, M. Tahir, P. Wu, L. Mai, *Small Methods* **2021**, *5*, 2100508; b) T. Hou, W. Xu, X. Pei, L. Jiang, O. M. Yaghi, K. A. Persson, *J. Am. Chem. Soc.* **2022**, *144*, 13446.

[10] P. Zhou, X. Zhang, Y. Xiang, K. Liu, *Nano Res.* **2022**, *16*, 8055.

[11] a) K. Xu, *Chem. Rev.* **2004**, *104*, 4303; b) Z. Hao, C. Wang, Y. Wu, Q. Zhang, H. Xu, Y. Jin, J. Liu, H. Wang, X. He, *Adv. Energy Mater.* **2023**, *13*, 2204007; c) Y. Li, S. Ma, Y. Zhao, S. Chen, T. Xiao, H. Yin, H. Song, X. Pan, L. Cong, H. Xie, *Energy Environ. Mater.* **2024**, *7*, 12648.

[12] a) L. Xu, X. Xiao, H. Tu, F. Zhu, J. Wang, H. Liu, W. Huang, W. Deng, H. Hou, T. Liu, X. Ji, K. Amine, G. Zou, *Adv. Mater.* **2023**, *35*, 2303193; b) P. Dong, X. Zhang, W. Hiscox, J. Liu, J. Zamora, X. Li, M. Su, Q. Zhang, X. Guo, J. McCloy, M.-K. Song, *Adv. Mater.* **2023**, *35*, 2211841; c) Y. Xu, Z. Chen, J. Wang, B. Li, J. Li, Z. He, L. Li, L. Gao, S. Han, J. Bian, J. Zhu, L. Wang, Y. Zhao, Q. Xu, R. Zhao, *Angew. Chem., Int. Ed.* **2025**, *64*, 202416170; d) X. Song, K. Ma, J. Wang, H. Wang, H. Xie, Z. Zheng, J. Zhang, *ACS Nano* **2024**, *18*, 12311.

[13] a) H. Liu, H. Pan, M. Yan, X. Zhang, Y. Jiang, *Adv. Mater.* **2023**, *35*, 2300888; b) Z. Li, S. Wang, J. Shi, Y. Liu, S. Zheng, H. Zou, Y. Chen, W. Kuang, K. Ding, L. Chen, Y.-q. Lan, Y.-p. Cai, Q. Zheng, *Energy Storage Mater.* **2022**, *47*, 262.

[14] a) K. Tang, Q. Bai, P. Xu, R. Liu, S. Xue, S. Liu, Y. Zhu, *Small Methods* **2024**, *8*, 2301810; b) Y. Zhou, J. Chen, J. Sun, T. Zhao, *Nano Lett.* **2024**, *24*, 2033; c) M. C. Nguyen, H. L. Nguyen, T. P. M. Duong, S.-H. Kim, J.-Y. Kim, J.-H. Bae, H.-K. Kim, S. N. Lim, W. Ahn, *Adv. Funct. Mater.* **2024**, *34*, 2406987.

[15] a) J. Zhang, Y. Wang, Q. Xia, X. Li, B. Liu, T. Hu, M. Tebyetekerwa, S. Hu, R. Knibbe, S. Chou, *Angew. Chem., Int. Ed.* **2024**, *63*, 202318822; b) X.-X. Wang, D.-H. Guan, C.-L. Miao, D.-C. Kong, L.-J. Zheng, J.-J. Xu, *J. Am. Chem. Soc.* **2023**, *145*, 5718; c) W. Xu, X. Pei, C. S. Diercks, H. Lyu, Z. Ji, O. M. Yaghi, *J. Am. Chem. Soc.* **2019**, *141*, 17522.

[16] T. D. Bennett, S. Horike, J. C. Mauro, M. M. Smedskjaer, L. Wondraczek, *Nat. Chem.* **2024**, *16*, 1755.

[17] a) M. Sun, J. Li, H. Yuan, X. Zeng, J. Lan, Y. Yu, X. Yang, *Mater. Today Energy* **2022**, *29*, 101117; b) R. Lin, M. Chai, Y. Zhou, V. Chen, T. D. Bennett, J. Hou, *Chem. Soc. Rev.* **2023**, *52*, 4149; c) M. Chai, R. Chen, K. Xu, Y. Chen, S. Ma, R. Lin, V. Chen, J. Hou, *J. Mater. Chem. A* **2023**, *11*, 20302.

[18] a) R. Garcia-Mendez, J. G. Smith, J. C. Neuefeind, D. J. Siegel, J. Sakamoto, *Adv. Energy Mater.* **2020**, *10*, 2000335; b) H. Su, Y. Zhong, C. Wang, Y. Liu, Y. Hu, J. Li, M. Wang, L. Jiao, N. Zhou, B. Xiao, X. Wang, X. Sun, J. Tu, *Nat. Commun.* **2024**, *15*, 2552; c) T. Dai, S. Wu, Y. Lu, Y. Yang, Y. Liu, C. Chang, X. Rong, R. Xiao, J. Zhao, Y. Liu, W. Wang, L. Chen, Y.-S. Hu, *Nat. Energy* **2023**, *8*, 1221.

© 2025 Wiley-VCH GmbH

16163028, 0, Downloaded from https://advanced.onlinelibrary.wiley.com/doi/10.1002/adfm.202505700 by Northwestern Polytechnic, Wiley Online Library on [29/05/2025]. See the Terms and Conditions (https://onlinelibrary.wiley.com/terms-and-conditions) on Wiley Online Library for rules of use; OA articles are governed by the applicable Creative Commons License

16163028, 0, Downloaded from https://advanced.onlinelibrary.wiley.com/doi/10.1002/adfm.202505700 by Northwestern Polytechnic, Wiley Online Library on [29/05/2025]. See the Terms and Conditions (https://onlinelibrary.wiley.com/terms-and-conditions) on Wiley Online Library for rules of use; OA articles are governed by the applicable Creative Commons License

[19] O. Kong, G. Jiang, K. Wang, A. Yang, J. Zheng, S. Wu, W. Han, J. Li, L. Li, X. An, J. Wang, C. Sun, L. Li, F. Xu, B. An, *Adv. Energy Mater.* **2025**, https://doi.org/10.1002/aenm.202405593.

[20] a) X. X. Wang, D. H. Guan, C. L. Miao, J. X. Li, J. Y. Li, X. Y. Yuan, X. Y. Ma, J. J. Xu, *Adv. Energy Mater.* **2024**, *14*, 2303829; b) J. Ding, T. Du, E. H. Thomsen, D. Andresen, M. R. Fischer, A. K. Moller, A. R. Petersen, A. K. Pedersen, L. R. Jensen, S. Wang, M. M. Smedskjaer, *Adv. Sci.* **2024**, *11*, 2306698; c) Y. Zhang, Y. Liu, W. Bao, X. Zhang, P. Yan, X. Yao, M. Z. Chen, T. Y. Xie, L. Cao, X. Cai, H. Li, Y. Deng, L. Zhao, M. H. Zeng, S. Jiang, Y. Zhao, J. Xie, *Nano Lett.* **2023**, *23*, 4066.

[21] a) H. Z. Tao, T. D. Bennett, Y. Z. Yue, *Adv. Mater.* **2017**, *29*, 1601705; b) B. Li, C. Wang, R. Yu, J. Han, S. Jiang, C. Zhang, S. He, *Energy Environ. Sci.* **2024**, *17*, 1854.

[22] a) Y. Ni, L. Lin, Y. Shang, L. Luo, L. Wang, Y. Lu, Y. Li, Z. Yan, K. Zhang, F. Cheng, J. Chen, *Angew. Chem., Int. Ed.* **2021**, *60*, 16937; b) S. Yao, X. Zhao, X. Wan, X. Wang, T. Huang, J. Zhang, L. Li, *Mater. Horiz.* **2021**, *8*, 3457.

[23] J. Hou, M. L. Rios Gomez, A. Krajnc, A. McCaul, S. Li, A. M. Bumstead, A. F. Sapnik, Z. Deng, R. Lin, P. A. Chater, D. S. Keeble, D. A. Keen, D. Appadoo, B. Chan, V. Chen, G. Mali, T. D. Bennett, *J. Am. Chem. Soc.* **2020**, *142*, 3880.

[24] W. L. Xue, C. Das, J. B. Weiß, S. Henke, *Angew. Chem., Int. Ed.* **2024**, *63*, 202405307.

[25] Z. Yang, Y. Belmabkhout, L. N. McHugh, D. Ao, Y. Sun, S. Li, Z. Qiao, T. D. Bennett, M. D. Guiver, C. Zhong, *Nat. Mater.* **2023**, *22*, 888

[26] O. Smirnova, S. Hwang, R. Sajzew, L. Ge, A. Reupert, V. Nozari, S. Savani, C. Chmelik, M. R. Reithofer, L. Wondraczek, J. Karger, A. Knebel, *Nat. Mater.* **2024**, *23*, 262.

[27] T. Du, X. Ge, F. Cao, H. Liu, C. Shi, J. Ding, D. Sun, Q. Zhang, Y. Yue, M. M. Smedskjaer, *Chem. Mater.* **2024**, *36*, 6167.

[28] A. M. Bumstead, M. L. Ríos Gómez, M. F. Thorne, A. F. Sapnik, L. Longley, J. M. Tuffnell, D. S. Keeble, D. A. Keen, T. D. Bennett, *CrystEngComm* **2020**, *22*, 3627.

[29] Q. Lv, C. Li, Y. Liu, Y. Jing, J. Sun, H. Wang, L. Wang, H. Ren, B. Wu, T. Cheng, D. Wang, H. Liu, S.-X. Dou, B. Wang, J. Wang, *ACS Nano* **2024**, *18*, 23253.

[30] S. Liu, G. Jiang, Y. Wang, C. Liu, T. Zhang, Y. Wei, B. An, *ACS Nano* **2024**, *18*, 14907.

[31] a) N. Wang, M. Jia, Z. Bi, X. Guo, *Adv. Funct. Mater.* **2024**, *34*, 2401400; b) Y. Nikodimos, S.-K. Jiang, S.-J. Huang, B. W. Taklu, W.-KongH. Huang, G. B. Desta, T. M. Tekaligne, Z. B. Muche, K. Lakshmanan, C.-Y. Chang, T. M. Hagos, K. N. Shitaw, S.-C. Yang, S.-H. Wu, W.-N. Su, B. J. Hwang, *ACS Energy Lett.* **2024**, *9*, 1844; c) S. Wang, X. Xu, C. Cui, C. Zeng, J. Liang, J. Fu, R. Zhang, T. Zhai, H. Li, *Adv. Funct. Mater.* **2022**, *32*, 2108805.

[32] a) Z. Li, L. Sun, L. Zhai, K. S. Oh, J. M. Seo, C. Li, D. Han, J. B. Baek, S. Y. Lee, *Angew. Chem., Int. Ed.* **2023**, *62*, 202307459; b) P. Liu, L. Miao, Z. Sun, X. Chen, Y. Si, Q. Wang, L. Jiao, *Angew. Chem., Int. Ed.* **2023**, *62*, 202312413.

[33] a) G. M. Hobold, C. Wang, K. Steinberg, Y. Li, B. M. Gallant, *Nat. Energy* **2024**, *9*, 580; b) H. Zeng, K. Yu, J. Li, M. Yuan, J. Wang, Q. Wang, A. Lai, Y. Jiang, X. Yan, G. Zhang, H. Xu, J. Wang, W. Huang, C. Wang, Y. Deng, S.-S. Chi, *ACS Nano* **2024**, *18*, 1969; c) J. Zhang, S. Li, X. Wang, S. Mao, J. Guo, Z. Shen, J. Mao, Q. Wu, K. Shen, H. Cheng, Y. Tan, Y. Lu, *Adv. Energy Mater.* **2024**, *14*, 2302587.

[34] X. Xu, J. Chen, J. Li, Z. Wang, J. Shen, P. Lin, J. Sun, B. Huang, T. Zhao, *Adv. Funct. Mater.* **2025**, *35*, 2415298.

[35] F. Pei, L. Wu, Y. Zhang, Y. Liao, Q. Kang, Y. Han, H. Zhang, Y. Shen, H. Xu, Z. Li, Y. Huang, *Nat. Commun.* **2024**, *15*, 351.

© 2025 Wiley-VCH GmbH